

The method of images for regularized Stokeslets

Josephine Ainley^a, Sandra Durkin^b, Rafael Embid^c,
Priya Boindala^c, Ricardo Cortez^{c,*}

^a *Mathematics Department, Southern University of Baton Rouge, United States*

^b *The University of Michigan, United States*

^c *Mathematics Department, Tulane University, 6823 Saint Charles Avenue, 424, New Orleans, LA 70118, United States*

Received 2 July 2007; received in revised form 8 January 2008; accepted 14 January 2008

Available online 2 February 2008

Abstract

The image system for the method of regularized Stokeslets is developed and implemented. The method uses smooth localized functions to approximate a delta distribution in the derivation of the fluid flow due to a concentrated force. In order to satisfy zero-flow boundary conditions at a plane wall, the method of images derived for a standard (singular) Stokeslet is extended to give exact cancellation of the regularized flow at the wall. As the regularization parameter vanishes, the expressions reduce to the known images for singular Stokeslets. The advantage of the regularized method is that it gives bounded velocity fields even for isolated forces or for distributions of forces along curves. These are useful in the simulation of ciliary beats, flagellar motion, and particle suspensions. The expression relating force and velocity can be inverted to find the forces that generate a given velocity boundary condition. The latter is exemplified by modeling a cilium as a filament moving in a three-dimensional flow. The cilium velocity at various times is constructed from known data and used to determine the force field along the filament. Those forces can then reproduce the flow everywhere. The validity of the method is evaluated by computing the drag on a sphere moving near a wall. Comparisons with known expressions for the drag show that the method gives accurate results for spheres even within a distance from the wall equal to the surface discretization size.

© 2008 Elsevier Inc. All rights reserved.

MSC: 76D07; 35Q30

Keywords: Stokeslet; Method of images

1. Introduction

Microscopic flows involved in the dynamics of swimming organisms, beating cilia and minute particles are modeled adequately with the Stokes equations, which are valid in the limit of zero Reynolds number. Many of these situations require understanding the fluid motion near a plane wall, where boundary conditions must be

* Corresponding author. Tel.: +1 504 862 3436; fax: +1 504 865 5063.

E-mail addresses: sjdurkin@umich.edu (S. Durkin), rembid@gmail.com (R. Embid), pboindal@tulane.edu (P. Boindala), cortez@tulane.edu (R. Cortez).

satisfied. Experimental measurements of the motion of bacteria near the bottom of a glass plate, for example, include the effect of the glass wall. The motion of cilia is affected by the membrane where the cilia are attached. For the numerical simulation of flows near a plane wall, investigators have used the method of images (or reflections) to satisfy the zero-velocity condition at the wall. Lorentz in 1907 first computed the flow due to a singular point force located above a plane wall in a small-Reynolds number flow. Blake [5] used Fourier transforms to derive the flow due to a Stokeslet near an infinite plane wall.

The idea of those methods is to identify the mirror image across the wall of the point where the force on the fluid is exerted, and apply more singular solutions of the Stokes equations at the image point, which lies outside the fluid domain. The correct linear combination of the singularity solutions satisfies the boundary conditions. This approach has been very useful for computational models of solid bodies moving near a plane, where there is a force distribution on the surface of the body. For surface distributions of Stokeslets, the resulting velocity expression is an integrable kernel that can be computed with careful quadratures. The images are typically outside the fluid domain where their higher singularities do not present a problem.

However, there is an increasing number of applications that result in a non-integrable kernel. Examples are Stokeslets distributions along filaments in three dimensions resulting in a line integral of the Greens function, and forces applied to the fluid at scattered points which is a superposition of singular solutions without an integral representation. These situations arise from models of ciliary beats, flagellar motion, and particle suspensions. A class of numerical methods designed to deal with the singularities includes the immersed boundary method [30,14], the blob projection method [12], and the method of regularized Stokeslets [10,11]. They use regularized (or approximate) delta functions that have the effect of smoothing out the force and spreading it to a small volume surrounding the filament or points of application. Similar regularization methods are common for fast fluid motions; the most popular being the vortex blob method developed by Chorin [7]. Since then, there has been much work on designing blobs with desired properties (see [19,2,1]).

Blake’s system of images for the singular Stokeslet does not exactly cancel the regularized flows at the wall, especially when the forces are applied close to the wall. Therefore, the need arises to adapt the system of images to be used with the regularization methods. In this paper we derive the system of images for the method of regularized Stokeslets in three dimensions to flows bounded by an infinite wall. The image system is an extension of the one developed by Blake [5], also discussed in [31], but takes into account the regularization of the forces. The images require those of the original (singular) case plus an additional element that arises from the regularization. Both, the singular and the regularized cases are presented in order to show clearly where the derivations differ. The result is an explicit formula relating the fluid velocity and the forces generating the flow. This expression is linear and can be inverted to solve for the forces that generate a given velocity. Several examples from biology are presented to display the use of the method in applications, particularly the motility of microorganisms and the motion of cilia.

2. Background and equations

The velocity and pressure in the fluid are found by solving the time-independent incompressible Stokes equations in three dimensions

$$\mu\Delta\mathbf{U} = \nabla p - \mathbf{F}(\mathbf{x}), \tag{1}$$

$$\nabla \cdot \mathbf{U} = 0, \tag{2}$$

where μ is the viscosity, \mathbf{U} is the velocity of the fluid, p is the pressure, and \mathbf{F} is the external force. If we let \mathbf{f} be a constant vector coefficient and we assume the external force is given by a point force $\mathbf{F}(\mathbf{x}) = \mathbf{f}\delta(\mathbf{x} - \mathbf{x}_0)$, the *Stokeslet* is the velocity \mathbf{U}_s that satisfies these equations for that forcing. The expressions for the Stokeslet and corresponding pressure are

$$p(\mathbf{x}) = -\frac{\mathbf{f} \cdot (\mathbf{x} - \mathbf{x}_0)}{4\pi r^3},$$

$$\mu\mathbf{U}_s(\mathbf{x}) = \frac{\mathbf{f}}{8\pi r} + \frac{(\mathbf{f} \cdot (\mathbf{x} - \mathbf{x}_0))(\mathbf{x} - \mathbf{x}_0)}{8\pi r^3},$$

where $r = |\mathbf{x} - \mathbf{x}_0|$.

The method of regularized Stokeslets assumes the force is not a Dirac delta applied at a single point but uses a shape function, such as a Gaussian, that modulates how the force is distributed spatially in a small ball around a point \mathbf{x}_0 . The shape functions are usually called *blobs* and a parameter δ determines the spread of the blob. The result of this approach is that for $\delta > 0$, the resulting expressions for the regularized Stokeslet contain no singularities. The velocity is finite everywhere and it approximates the standard Stokeslet away from the force [11].

We use the notation

$$\psi_\delta(r) = \frac{1}{\delta^3} \psi(r/\delta)$$

to represent a scaled version of a smooth radial function $\psi(r)$ that satisfies $4\pi \int_0^\infty r^2 \psi(r) dr = 1$. The function $\psi(r)$ may be any smooth function concentrated near $r = 0$. Note that

$$\lim_{\delta \rightarrow 0} \psi_\delta(r) = \delta(r).$$

We now assume the force is given by $\mathbf{F}(\mathbf{x}) = \mathbf{f}\psi_\delta(|\mathbf{x} - \mathbf{x}_0|)$ and derive the exact solution of the Stokes equations for this forcing. Let the domain be all of \mathbb{R}^3 , take the divergence of Eq. (1) and use Eq. (2) to get $\Delta p_s = \mathbf{f} \cdot \nabla \psi_\delta$. This gives

$$p_s(\mathbf{x}) = \mathbf{f} \cdot \nabla G_\delta(|\mathbf{x} - \mathbf{x}_0|), \tag{3}$$

where the *regularized Green’s function* satisfies $\Delta G_\delta = \psi_\delta$. We now substitute this expression into Eq. (1) and get

$$\mu \Delta \mathbf{U} = (\mathbf{f} \cdot \nabla) \nabla G_\delta - \mathbf{f} \psi_\delta$$

from which we deduce that

$$\mu \mathbf{U}_s(\mathbf{x}) = (\mathbf{f} \cdot \nabla) \nabla B_\delta(|\mathbf{x} - \mathbf{x}_0|) - \mathbf{f} G_\delta(|\mathbf{x} - \mathbf{x}_0|), \tag{4}$$

where the *regularized biharmonic* function satisfies $\Delta B_\delta = G_\delta$. Due to the linearity of the Stokes equations, the superposition of Stokeslets is also a solution of the equations. For notational purposes, we will write $\mathbf{U}_s = S_\delta[\mathbf{f}]$ to indicate the flow due to a Stokeslet of constant strength \mathbf{f} .

It is important to emphasize that for $\delta > 0$, the regularized Stokeslet is a bounded flow for all \mathbf{x} , so that even the flow due to a single (regularized) force can be computed without singularities. At the same time, the standard singular Stokeslet can be recovered by simply taking the limit as $\delta \rightarrow 0$ of the expression in Eq. (4) regardless of the particular choice of blob ψ_δ .

Other more singular solutions of Stokes equations can be found by differentiating the regularized Stokeslet. In particular, since the force is localized near \mathbf{x}_0 , derivatives of the pressure and the velocity yield additional solutions of the equations. We explicitly derive the Stokeslet doublet, the potential dipole and the rotlet, which are needed in the remaining sections.

2.1. The Stokeslet doublet

The directional derivative of a Stokeslet, $(\mathbf{b} \cdot \nabla) \mathbf{U}_s$, in the direction of a constant vector \mathbf{b} is called the Stokeslet doublet (or simply doublet). Specifically, for a Stokeslet of strength \mathbf{g} , we will write

$$\mathbf{U}_{sd}(\mathbf{x}) = SD_\delta[\mathbf{g}, \mathbf{b}] = (\mathbf{b} \cdot \nabla)(\mathbf{g} \cdot \nabla) \nabla B_\delta(|\mathbf{x} - \mathbf{x}_0|) - \mathbf{g}(\mathbf{b} \cdot \nabla) G_\delta(|\mathbf{x} - \mathbf{x}_0|). \tag{5}$$

In the image system, the vector \mathbf{b} will be chosen as a function of \mathbf{g} in order to cancel components of the velocity at the wall.

2.2. The potential dipole

The potential dipole is the flow obtained by applying the negative Laplacian to \mathbf{U}_s . For an arbitrary constant force \mathbf{q} , this gives

$$\mathbf{U}_{pd}(\mathbf{x}) = PD_\delta[\mathbf{q}] = \mathbf{q} \psi_\delta(|\mathbf{x} - \mathbf{x}_0|) - (\mathbf{q} \cdot \nabla) \nabla G_\delta(|\mathbf{x} - \mathbf{x}_0|), \tag{6}$$

where \mathbf{q} will be selected appropriately to cancel the velocity at the wall.

2.3. The rotlet

Finally, there is one more element that will be needed in the system of images for the regularized Stokeslet. This element is not needed in the singular system of images since it is proportional to δ^2 and thus vanishes as $\delta \rightarrow 0$. A rotlet of constant strength \mathbf{L} is the antisymmetric part of the Stokeslet doublet and is defined as [17]

$$\mathbf{U}_r(\mathbf{x}) = R_\delta[\mathbf{L}] = \mathbf{L} \times \nabla G_\delta(|\mathbf{x} - \mathbf{x}_0|). \tag{7}$$

3. The method of images in the singular case

Blake [5] derived the image system for a (singular) Stokeslet based on Fourier transforms (see also Pozrikidis [31]). We rederive it here in a different way which will extend to the regularized case. All the expressions needed here are the ones that result from taking the limit $\delta \rightarrow 0$ in the previous section. The results follow from the functions

$$\lim_{\delta \rightarrow 0} G_\delta(r) = G(r) = -\frac{1}{4\pi r} \quad \text{and} \quad \lim_{\delta \rightarrow 0} B_\delta(r) = B(r) = -\frac{r}{8\pi}.$$

Based on these expressions, one finds that in the singular case

$$\mathbf{U}_s(\mathbf{x}) = S[\mathbf{f}] = \frac{\mathbf{f}}{8\pi r} + \frac{(\mathbf{f} \cdot (\mathbf{x} - \mathbf{x}_0))(\mathbf{x} - \mathbf{x}_0)}{8\pi r^3}, \tag{8}$$

$$\mathbf{U}_{pd}(\mathbf{x}) = PD[\mathbf{q}] = \frac{\mathbf{q}}{4\pi r^3} - 3 \frac{(\mathbf{q} \cdot (\mathbf{x} - \mathbf{x}_0))(\mathbf{x} - \mathbf{x}_0)}{4\pi r^5} \tag{9}$$

$$\begin{aligned} \mathbf{U}_{sd}(\mathbf{x}) &= SD[\mathbf{g}, \mathbf{b}] \\ &= \frac{(\mathbf{g} \cdot \mathbf{b})(\mathbf{x} - \mathbf{x}_0)}{8\pi r^3} + \frac{(\mathbf{g} \cdot (\mathbf{x} - \mathbf{x}_0))\mathbf{b}}{8\pi r^3} - \frac{(\mathbf{b} \cdot (\mathbf{x} - \mathbf{x}_0))\mathbf{g}}{8\pi r^3} - \frac{3(\mathbf{g} \cdot (\mathbf{x} - \mathbf{x}_0))(\mathbf{b} \cdot (\mathbf{x} - \mathbf{x}_0))(\mathbf{x} - \mathbf{x}_0)}{8\pi r^5}. \end{aligned} \tag{10}$$

We consider the fluid domain to be the half space of all points (x, y, z) with $x > w$, where $x = w$ is the plane (a wall) where the flow must vanish (see Fig. 1). Let a Stokeslet of strength \mathbf{f} be centered at $\mathbf{x}_0 = (w + h, y, z)$ in the fluid domain ($h > 0$). Here h represents the distance of the point force from the wall. The illusion of a wall at $x = w$ is created by introducing other elements at the image $\mathbf{x}_{0,im}$ reflected across the wall. The image point is $\mathbf{x}_{0,im} = (w - h, y, z)$ so that $\mathbf{x}_0 = \mathbf{x}_{0,im} + 2h\mathbf{e}_1$.

To evaluate the flow at an arbitrary point \mathbf{x}_e on the wall we define $\mathbf{x}^* = \mathbf{x}_e - \mathbf{x}_0$ and $\mathbf{x} = \mathbf{x}_e - \mathbf{x}_{0,im}$. Given the Stokeslet \mathbf{f} at \mathbf{x}_0 , we first place a Stokeslet of strength $-\mathbf{f}$ at the image point $\mathbf{x}_{0,im}$. Since $|\mathbf{x}^*| = |\mathbf{x}| = r$ we have that the flow due to the two Stokeslets at the wall is

$$\mathbf{U}_s(\mathbf{x}_e) - \mathbf{U}_{s,im}(\mathbf{x}_e) = \frac{\mathbf{f}}{8\pi r} + \frac{(\mathbf{f} \cdot \mathbf{x}^*)\mathbf{x}^*}{8\pi r^3} - \frac{\mathbf{f}}{8\pi r} - \frac{(\mathbf{f} \cdot \mathbf{x})\mathbf{x}}{8\pi r^3}.$$

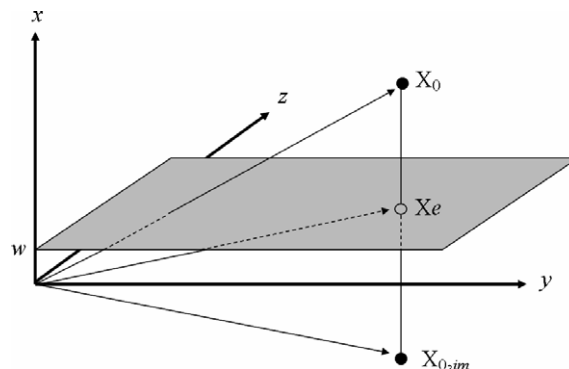


Fig. 1. Schematic of the fluid domain with the wall at $x = w$, the location of the Stokeslet at \mathbf{x}_0 and the image point.

Now we use the relation $\mathbf{x}^* = \mathbf{x} - 2h\mathbf{e}_1$ to find

$$\mathbf{U}_s(\mathbf{x}_e) - \mathbf{U}_{s,\text{im}}(\mathbf{x}_e) = \frac{-2h(\mathbf{f} \cdot \mathbf{x})\mathbf{e}_1 - 2hf_1\mathbf{x} + 4h^2f_1\mathbf{e}_1}{8\pi r^3}.$$

The negative Stokeslet at the image point has cancelled some of the velocity at the wall, but terms of $O(h)$ remain. We can simplify this expression slightly to see that the components of the velocity are

$$\mathbf{U}_s(\mathbf{x}_e) - \mathbf{U}_{s,\text{im}}(\mathbf{x}_e) = \frac{-2h}{8\pi r^3} \begin{pmatrix} f_2y + f_3z \\ f_1y \\ f_1z \end{pmatrix}. \tag{11}$$

We seek to cancel these terms by considering a combination of a dipole and a doublet. In Eq. (10), we make the specific choice $\mathbf{g} = \mathbf{e}_1 = (1, 0, 0)$ and simplify to get

$$\mathbf{U}_{\text{sd}}(\mathbf{x}_e) = \text{SD}[\mathbf{e}_1, \mathbf{b}] = \frac{b_1\mathbf{x}}{8\pi r^3} + \frac{h\mathbf{b}}{8\pi r^3} - \frac{(\mathbf{b} \cdot \mathbf{x})\mathbf{e}_1}{8\pi r^3} - \frac{3h(\mathbf{b} \cdot \mathbf{x})\mathbf{x}}{8\pi r^5}. \tag{12}$$

If we now choose the dipole strength in Eq. (9) to be $\mathbf{q} = -\frac{1}{2}h\mathbf{b}$, we see that the dipole cancels part of the doublet. With these choices, we add the two contributions to get

$$\mathbf{U}_{\text{pd}}(\mathbf{x}_e) + \mathbf{U}_{\text{sd}}(\mathbf{x}_e) = \frac{b_1\mathbf{x}}{8\pi r^3} - \frac{(\mathbf{b} \cdot \mathbf{x})\mathbf{e}_1}{8\pi r^3} = \frac{-1}{8\pi r^3} \begin{pmatrix} b_2y + b_3z \\ -b_1y \\ -b_1z \end{pmatrix}. \tag{13}$$

Comparing Eq. (13) with Eq. (11) we see that the choice $(b_1, b_2, b_3) = 2h(f_1, -f_2, -f_3)$ leads to complete cancellation of the fluid velocity at all points on the wall $x_e = w$.

In summary, the image system for a singular Stokeslet of strength \mathbf{f} consists of a Stokeslet, a potential dipole and a Stokeslet doublet

$$-S[\mathbf{f}] - h^2\text{PD}[\mathbf{g}] + 2h\text{SD}[\mathbf{e}_1, \mathbf{g}],$$

where $\mathbf{g} = (g_1, g_2, g_3) = (f_1, -f_2, -f_3) = 2(\mathbf{f} \cdot \mathbf{e}_1)\mathbf{e}_1 - \mathbf{f}$.

As described in the Introduction, this system of images for the singular Stokeslet does not directly apply to models that makes use of single forces at scattered points or force distributions along curves in three dimensions. The resulting expressions are too singular for the velocities to be bounded at the force locations. This motivates the use of regularization technique introduced in the previous section that modifies the forces from being applied at a single point to being concentrated in a small sphere around the point. The system of images for the regularized expressions is presented next.

4. The regularized image system

In the regularized case, the velocity expressions can be written as

$$\mathbf{U}_s(\mathbf{x}) = S_\delta[\mathbf{f}] = \mathbf{f}H_1(r) + (\mathbf{f} \cdot (\mathbf{x} - \mathbf{x}_0))(\mathbf{x} - \mathbf{x}_0)H_2(r),$$

$$\mathbf{U}_{\text{pd}}(\mathbf{x}) = \text{PD}_\delta[\mathbf{q}] = \mathbf{q}D_1(r) + (\mathbf{q} \cdot (\mathbf{x} - \mathbf{x}_0))(\mathbf{x} - \mathbf{x}_0)D_2(r),$$

$$\begin{aligned} \mathbf{U}_{\text{sd}}(\mathbf{x}) = \text{SD}_\delta[\mathbf{g}, \mathbf{b}] &= (\mathbf{g} \cdot \mathbf{b})(\mathbf{x} - \mathbf{x}_0)H_2(r) + (\mathbf{g} \cdot (\mathbf{x} - \mathbf{x}_0))\mathbf{b}H_2(r) + (\mathbf{b} \cdot (\mathbf{x} - \mathbf{x}_0))\mathbf{g}\frac{H'_1(r)}{r} \\ &+ (\mathbf{g} \cdot (\mathbf{x} - \mathbf{x}_0))(\mathbf{b} \cdot (\mathbf{x} - \mathbf{x}_0))(\mathbf{x} - \mathbf{x}_0)\frac{H'_2(r)}{r}, \end{aligned}$$

where the functions $H_1(r)$, $H_2(r)$, $D_1(r)$ and $D_2(r)$ come from the formulas in Eqs. (4)–(6) and provide the regularization to the velocity. They depend exclusively on the blob used. Since $\Delta G_\delta(r) = \psi_\delta(r)$ and $\Delta B_\delta(r) = G_\delta(r)$, we can write

$$H_1(r) = \frac{B'_\delta}{r} - G_\delta, \quad H_2(r) = \frac{rB''_\delta - B'_\delta}{r^3}, \tag{14}$$

$$D_1(r) = \frac{G'_\delta}{r} - \psi_\delta, \quad D_2(r) = \frac{rG''_\delta - G'_\delta}{r^3}. \tag{15}$$

One can easily verify that in the limit as $\delta \rightarrow 0$, these functions reduce to the singular case discussed in the previous section. Note that the Stokeslet doublet has been written using the same functions $H_1(r)$ and $H_2(r)$ that appear in the Stokeslet since we derived the doublet by differentiating the Stokeslet.

Proceeding as before, we place a Stokeslet of strength $-\mathbf{f}$ at the image point, let \mathbf{x}_e be any point on the wall and define $\mathbf{x}^* = \mathbf{x}_e - \mathbf{x}_0$ and $\mathbf{x} = \mathbf{x}_e - \mathbf{x}_{0,im}$. We use the relation $\mathbf{x}^* = \mathbf{x} - 2h\mathbf{e}_1$ to find

$$\mathbf{U}_s(\mathbf{x}_e) - \mathbf{U}_{s,im}(\mathbf{x}_e) = [-2h(\mathbf{f} \cdot \mathbf{x})\mathbf{e}_1 - 2hf_1\mathbf{x} + 4h^2f_1\mathbf{e}_1] H_2(r)$$

which simplifies to

$$\mathbf{U}_s(\mathbf{x}_e) - \mathbf{U}_{s,im}(\mathbf{x}_e) = -2hH_2(r) \begin{pmatrix} f_2y + f_3z \\ f_1y \\ f_1z \end{pmatrix}. \tag{16}$$

We now continue with the combination of a potential dipole and the Stokeslet doublet. Based on the singular expression, we let the strength of the dipole be $\mathbf{q} = -\frac{1}{2}h\mathbf{b}$ and we find

$$-\frac{h}{2}PD_\delta[\mathbf{b}] + SD_\delta[\mathbf{e}_1, \mathbf{b}] = h\mathbf{b} \left[H_2(r) - \frac{1}{2}D_1(r) \right] + h(\mathbf{b} \cdot \mathbf{x})\mathbf{x} \left[\frac{H'_2(r)}{r} - \frac{1}{2}D_2(r) \right] + b_1\mathbf{x}H_2(r) + (\mathbf{b} \cdot \mathbf{x})\mathbf{e}_1 \frac{H'_1(r)}{r}. \tag{17}$$

In the singular case, the first two terms of the right side vanished. Here, the functions depend on the specific blob used so we expect that if we expand the expressions in brackets in powers of δ , the leading-order terms will cancel but there may be additional terms that remain. As an example, if we use the blob

$$\psi_\delta(r) = \frac{15\delta^4}{8\pi(r^2 + \delta^2)^{7/2}}, \tag{18}$$

we find that

$$\left[\frac{H'_2(r)}{r} - \frac{1}{2}D_2(r) \right] = \frac{15\delta^2}{16\pi(r^2 + \delta^2)^{7/2}}$$

which vanishes only when $\delta \rightarrow 0$ (and $r > 0$). However, we seek exact cancellation of the velocity at the wall in the presence of the regularization. More generally, we find that given a blob from a family of the form

$$\psi_\delta(r) = \frac{C_n\delta^{2n-2}}{4\pi(r^2 + \delta^2)^{n+1/2}}, \quad n \geq 2$$

the regularizing functions have similar denominators with different exponents. The largest exponent in the denominator of $D_2(r)$ is $n + 1/2$ while the largest exponent in the denominator of $H'_2(r)/r$ is only $n - 1/2$. This indicates that it is impossible for the expression $\frac{H'_2(r)}{r} - \frac{1}{2}D_2(r)$ to cancel if the regularizing functions are derived from the same blob of this family. However, the observation also means that if $H_1(r)$ and $H_2(r)$ are derived from the blob in Eq. (18) while the dipole function $D_1(r)$ and $D_2(r)$ are derived from a more slowly decaying blob

$$\phi_\delta(r) = \frac{3\delta^2}{4\pi(r^2 + \delta^2)^{5/2}}, \tag{19}$$

then the expression $\frac{H'_2(r)}{r} - \frac{1}{2}D_2(r)$ may cancel identically. In fact, we have the following result:

Proposition 1. *Let $H_1(r)$ and $H_2(r)$ be defined by Eq. (14) derived from the blob in Eq. (18) and let $D_1(r)$ and $D_2(r)$ be defined by Eq. (15) derived from the blob in Eq. (19). Then*

$$\frac{H'_2(r)}{r} - \frac{1}{2}D_2(r) = 0 \quad \text{and}$$

$$H_2(r) - \frac{1}{2}D_1(r) = -\frac{H_1'(r)}{r} - H_2(r).$$

Proof. Given the blob ψ_δ in Eq. (18), we compute the corresponding functions G_δ and B_δ from the relations $\Delta G_\delta = \psi_\delta$ and $\Delta B_\delta = G_\delta$. That is, we solve

$$G_\delta''(r) + \frac{2}{r}G_\delta'(r) = \psi_\delta \quad \text{and} \quad B_\delta''(r) + \frac{2}{r}B_\delta'(r) = G_\delta$$

and then use Eq. (14) to find $H_1(r)$ and $H_2(r)$. In the same manner but starting with the blob ϕ_δ in Eq. (19), we compute $D_1(r)$ and $D_2(r)$ from Eq. (15). The result follows from direct computation. \square

Going back to the linear combination of a regularized potential dipole and Stokeslet doublet in Eq. (17) and using the result of Proposition 1, we obtain the simpler expression

$$-\frac{h}{2}\text{PD}_\delta[\mathbf{b}] + \text{SD}_\delta[\mathbf{e}_1, \mathbf{b}] = -h\mathbf{b} \left[\frac{H_1'(r)}{r} + H_2(r) \right] + b_1\mathbf{x}H_2(r) + (\mathbf{b} \cdot \mathbf{x})\mathbf{e}_1 \frac{H_1'(r)}{r}.$$

As before, we let $\mathbf{b} = (b_1, b_2, b_3) = 2h(f_1, -f_2, -f_3)$ and simplify the previous expression to get

$$-\frac{h}{2}\text{PD}_\delta[\mathbf{b}] + \text{SD}_\delta[\mathbf{e}_1, \mathbf{b}] = -2h \frac{H_1'(r)}{r} \begin{pmatrix} f_2y + f_3z \\ 0 \\ 0 \end{pmatrix} + 2hH_2(r) \begin{pmatrix} 0 \\ f_1y \\ f_1z \end{pmatrix} + 2h^2 \left[\frac{H_1'(r)}{r} + H_2(r) \right] \begin{pmatrix} 0 \\ f_2 \\ f_3 \end{pmatrix}.$$

Adding this equation to Eq. (16) we have that

$$\mathbf{U}_s(\mathbf{x}_e) - \mathbf{U}_{s,\text{im}}(\mathbf{x}_e) - \frac{h}{2}\text{PD}_\delta[\mathbf{b}] + \text{SD}_\delta[\mathbf{e}_1, \mathbf{b}] = -2h \left[\frac{H_1'(r)}{r} + H_2(r) \right] \begin{pmatrix} f_2y + f_3z \\ -hf_2 \\ -hf_3 \end{pmatrix}. \tag{20}$$

The factor in brackets is

$$\frac{H_1'(r)}{r} + H_2(r) = \frac{-3\delta^2}{8\pi(r^2 + \delta^2)^{5/2}}$$

which vanishes only when $\delta \rightarrow 0$, as we know from the image system in the singular case. However, when $\delta > 0$ the images so far have not fully cancelled the flow at the wall. There is one additional element needed to satisfy the velocity boundary condition at the wall. The element is a combination of rotlets. To see this, notice that the expression in Eq. (20) is a cross product. If we define $\mathbf{L} = \mathbf{f} \times \mathbf{e}_1$ so that $(L_1, L_2, L_3) = (0, f_3, -f_2)$, then

$$\mathbf{L} \times \mathbf{x} = \begin{pmatrix} L_2z - L_3y \\ L_3x - L_1z \\ L_1y - L_2x \end{pmatrix} = \begin{pmatrix} f_2y + f_3z \\ -hf_2 \\ -hf_3 \end{pmatrix}.$$

Based on Eq. (7) and the fact that $\nabla G_\delta(\mathbf{x}) = \frac{G_\delta'(r)}{r}\mathbf{x}$, the need of rotlets is evident. It turns out that Eq. (20), represents exactly the flow due to the difference of two rotlets, one derived from the blob ψ_δ and the other from ϕ_δ in Eq. (19)

$$\mathbf{U}_r^\psi(\mathbf{x}_e) - \mathbf{U}_r^\phi(\mathbf{x}_e) = \mathbf{L} \times \left[\nabla G_\delta^\psi - \nabla G_\delta^\phi \right] = \frac{3\delta^2}{8\pi(r^2 + \delta^2)^{5/2}} (\mathbf{L} \times \mathbf{x})$$

so we conclude that the image system for a regularized Stokeslet (using ψ_δ) is

$$-S_\delta[\mathbf{f}] - h^2\text{PD}_\delta[\mathbf{g}] + 2h\text{SD}_\delta[\mathbf{e}_1, \mathbf{g}] + 2hR_\delta^\psi[\mathbf{L}] - 2hR_\delta^\phi[\mathbf{L}],$$

where $\mathbf{g} = 2(\mathbf{f} \cdot \mathbf{e}_1)\mathbf{e}_1 - \mathbf{f}$ and $\mathbf{L} = \mathbf{f} \times \mathbf{e}_1$.

In summary, given M regularized Stokeslets located at $\mathbf{x}_{k,0} = (w + h_k, y_k, z_k)$ in the fluid domain (i.e. $h_k > 0$), where $x = w$ is the wall, we define the image points to be $\mathbf{x}_{k,im} = (w - h_k, y_k, z_k)$. Let \mathbf{x}_e be the point where the fluid velocity is evaluated (not necessarily on the wall) and define $\mathbf{x}_k^* = \mathbf{x}_e - \mathbf{x}_{k,0}$ and $\mathbf{x}_k = \mathbf{x}_e - \mathbf{x}_{k,im}$. Then the velocity at \mathbf{x}_e is given by

$$\begin{aligned} \mathbf{U}(\mathbf{x}_e) = & \sum_{k=1}^M [\mathbf{f}_k H_1(|\mathbf{x}_k^*|) + (\mathbf{f}_k \cdot \mathbf{x}_k^*) \mathbf{x}_k^* H_2(|\mathbf{x}_k^*|)] - [\mathbf{f}_k H_1(|\mathbf{x}_k|) + (\mathbf{f}_k \cdot \mathbf{x}_k) \mathbf{x}_k H_2(|\mathbf{x}_k|)] - h_k^2 [\mathbf{g}_k D_1(|\mathbf{x}_k|) \\ & + (\mathbf{g}_k \cdot \mathbf{x}_k) \mathbf{x}_k D_2(|\mathbf{x}_k|)] - 2h_k \left[\frac{H_1'(|\mathbf{x}_k|)}{|\mathbf{x}_k|} + H_2(|\mathbf{x}_k|) \right] (\mathbf{L}_k \times \mathbf{x}_k) + 2h_k \left[(\mathbf{g}_k \cdot \mathbf{e}_1) \mathbf{x}_k H_2(|\mathbf{x}_k|) \right. \\ & \left. + (\mathbf{x}_k \cdot \mathbf{e}_1) \mathbf{g}_k H_2(|\mathbf{x}_k|) + (\mathbf{g}_k \cdot \mathbf{x}_k) \mathbf{e}_1 \frac{H_1'(|\mathbf{x}_k|)}{|\mathbf{x}_k|} + (\mathbf{x}_k \cdot \mathbf{e}_1) (\mathbf{g}_k \cdot \mathbf{x}_k) \mathbf{x}_k \frac{H_2'(|\mathbf{x}_k|)}{|\mathbf{x}_k|} \right], \end{aligned} \tag{21}$$

where the dipole strengths are $\mathbf{g}_k = 2(\mathbf{f}_k \cdot \mathbf{e}_1) \mathbf{e}_1 - \mathbf{f}_k$, the rotlet strengths are $\mathbf{L}_k = \mathbf{f}_k \times \mathbf{e}_1$ and

$$\begin{aligned} H_1(r) &= \frac{1}{8\pi(r^2 + \delta^2)^{1/2}} + \frac{\delta^2}{8\pi(r^2 + \delta^2)^{3/2}}, \\ H_2(r) &= \frac{1}{8\pi(r^2 + \delta^2)^{3/2}}, \\ D_1(r) &= \frac{1}{4\pi(r^2 + \delta^2)^{3/2}} - \frac{3\delta^2}{4\pi(r^2 + \delta^2)^{5/2}}, \\ D_2(r) &= -\frac{3}{4\pi(r^2 + \delta^2)^{5/2}}. \end{aligned}$$

5. Numerical examples

5.1. Example 1: flow due to two particles

We consider a representation of a swimming microorganism as two point forces located near each other but exerting opposite forces to the fluid. The *two-sphere model* is a simple model that has been used to understand the flow around a microorganism that has a cell body and flagella to propel itself [20]. The idea is that one sphere represents the cell body with instantaneous forward velocity while the second sphere represents roughly the tail as it sends a helical wave pushing the fluid backward. If the full geometry of the spheres is used, a boundary integral formulation can be used over the surface of the spheres. However, to model colonies with large numbers of microorganisms at coarser length scales, an efficient method would have to represent each organism by a small number of elements.

The two-sphere model is one that has been proposed to simulate the collective dynamics of swimming microorganisms [28,20]. In [20], the authors provide evidence that such a model can capture the dominant (leading-order) far field fluid dynamics which they argue is universal, regardless of the specific propulsion mechanism and swimmer shape. For zero net-force swimming, the far field is that of a force dipole (doublet). The simulated collective flow shows features such as wall-normal particle motion and large-scale coherent fluid motions at sufficiently high particle concentrations. Wall-normal motion has been observed in computations of a single organism composed of a cell body and a flagellum [16] as well as for polymer molecules [28]. The large-scale coherent fluid motion has been observed experimentally in organisms such as *Bacillus subtilis* [15]. We show in this section that these features are also reproduced by the simplified regularized Stokeslet model presented here.

We discuss a representation given by a pair of regularized Stokeslets. The regularization allows us to reduce each microorganism to a pair of points while maintaining a non-singular flow. Our motivation is that the far field flow due to a sphere with non-zero net surface force can be approximated by the flow produced by a single force at the center of the sphere; the magnitude of this force being equal to the net-force on the

sphere surface. The regularization parameter δ can give the length scale associated with the radius of each sphere.

In the first simple example, we consider a single organism represented by two particles located at the points where the blobs are centered. One particle has an instantaneous velocity U_0 parallel to the wall while the other has instantaneous velocity $-U_0$. In this case, we make the two regularization parameters equal to each other. In order to determine the Stokeslet strength at each particle location that would produce this velocity, we evaluate Eq. (21) at each particle location and solve the resulting 6×6 linear system of equations for the force components. Once the forces are known, the flow can be evaluated at any location with Eq. (21). Figs. 2 and 3 show the flow when the two points are located 0.1 units above the wall and 0.05 units apart from each other. The regularization parameter was set to $\delta = 0.05$. Fig. 2 shows a side view of the flow, including streamlines, and the effect of the wall. We point out the rotations above the organism that the forces create. Without the wall, these would exist all around the organism axisymmetrically. The wall, however, breaks the symmetry.

Fig. 3 shows top views of the flow in planes parallel to the wall. The middle figure shows the flow in a plane at the same height as the organism. The left and right figures show the flow at planes halfway between the organisms and wall, and twice as high as the organisms, respectively.

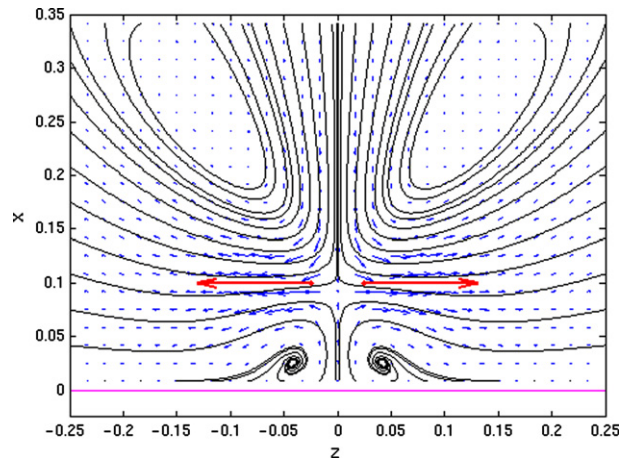


Fig. 2. Flow due to two particles moving away from each other parallel to the wall. The wall is at $x = 0$; the particles are 0.1 units above the wall and 0.05 units apart. The two thick arrows show the force at each particle; the other arrows are the flow field and the curves are streamlines. The regularization parameter was set to $\delta = 0.05$.

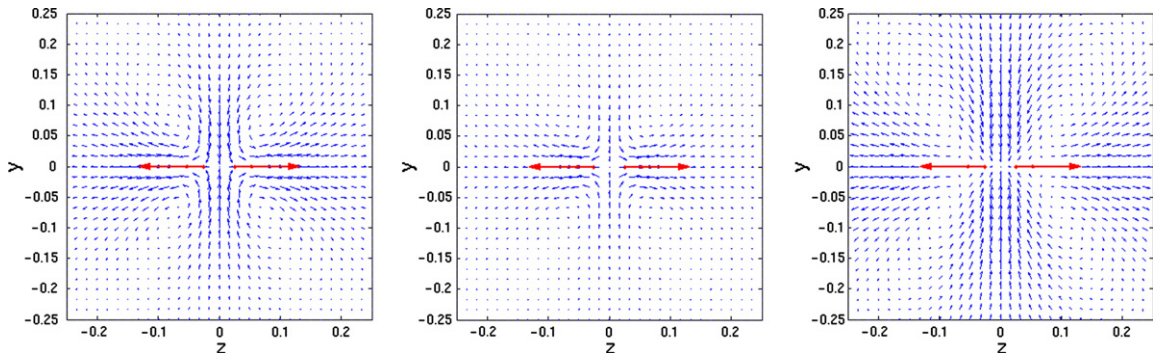


Fig. 3. Top view of the flow due to two particles moving away from each other parallel to the wall. The wall is at $x = 0$; the two particles are 0.1 units above the wall and 0.05 units apart. The two thick arrows show the force at each particle; the other arrows are the flow field. The left figure shows the flow at $x = 0.05$ (halfway between the wall and the particles). The middle figure shows the flow at the particle height. The right figure shows the flow at twice the particle height, $x = 0.2$. The regularization parameter was set to $\delta = 0.05$.

5.2. Example 2: the flow due to 25,000 organisms near a wall

Consider a wall located at $x = 0$ and a collection of 25,000 organisms (50,000 particles) placed randomly in the box $0 < x \leq 0.5$, $|y| \leq 0.25$ and $|z| \leq 0.5$. As in the previous example, each organism is represented by two particles oriented randomly in the domain; the organism length (particle separation) is $L = 0.02$. The two particles of each organism exert equal but opposite forces of unit magnitude on the fluid in the direction of the organism’s orientation. Such arrangement may be a simulation of the instantaneous flow generated by a colony of microorganisms moving under their own influence as well as that of the other organisms. Since each particle is represented by a single regularized Stokeslet, the regularization parameter δ provides a length scale that can be different for each particle. Such a representation would not be possible by singular Stokeslets. In this example the value was set to $\delta = 0.02$ for all particles. Fig. 4 shows the ‘cloud’ of particles and Fig. 5 shows the velocity field projected onto the plane $y = 0$. Each organism generates the flow of two Stokeslets which has features at a length scale comparable with the parameter L , the ‘size’ of the organism. However, large collections of particles tend to generate larger scale flows as seen in Fig. 5. In the figure, the length scale of the flow rotations are roughly 10 times larger than the particles themselves. This type of global flow is also observed experimentally [15,8].

5.3. Example 3: the motion of a cilium

The method of regularized Stokeslets with images can be used to understand the flow around a beating cilium. We model the cilium as a filament (curve) in three dimensions moving in a specified way. From a prescribed cilium velocity we find the forces along the points that define the cilium and we use the forces to compute the flow in the surrounding region. Here, we use an accurate representation of the cilium beat developed in [4] and reproduced in [18]. A point on the cilium at time t is parametrized by arclength s in a truncated Fourier series

$$\xi(s, t) = \frac{1}{2} \mathbf{a}_0(s) + \sum_{n=1}^{N_0} \mathbf{a}_n(s) \cos(n\sigma t) + \mathbf{b}_n(s) \sin(n\sigma t),$$

where $\xi = (\xi_1, \xi_2)$ lies in a plane. The coefficients $\mathbf{a}_n(s)$ and $\mathbf{b}_n(s)$ are cubic functions of s whose values are tabulated for $N_0 = 6$ (refer to [18]). By differentiating the cilium position $\xi(s, t)$ with respect to t , we find its instantaneous velocity. Eq. (21) is used then to solve for the force at each cilium point so that those points have the prescribed velocity. Finally, once the forces are known, the same formula in Eq. (21) is used to evaluate the flow around the cilium. The results of the power stroke are shown in Fig. 6 and those of the recovery stroke in Fig. 7. Not all 13 frames that the data in [18] provide are shown here, only four frames during the power stroke and four during the recovery stroke.

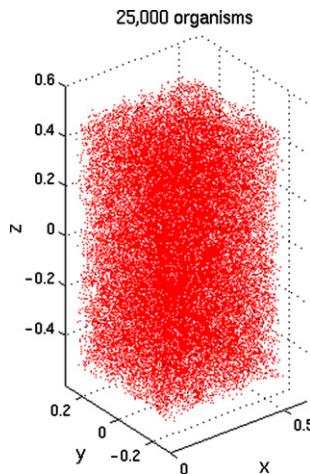


Fig. 4. Twenty-five thousands organisms (50,000 particles) randomly placed in the box $0 < x \leq 0.5$, $|y| \leq 0.25$ and $|z| \leq 0.5$.

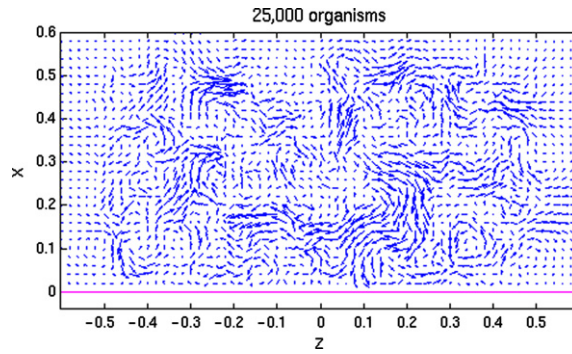


Fig. 5. Velocity field generated by 25,000 organisms (50,000 particles) randomly placed near the wall in the box $0 < x \leq 0.5$, $|y| \leq 0.25$ and $|z| \leq 0.5$. Two equal but opposite unit forces are exerted by each organism on the fluid in the direction of the organism’s orientation. The regularization parameter was set to $\delta = 0.02$. The figure shows the projection of the velocity on the plane $y = 0$.

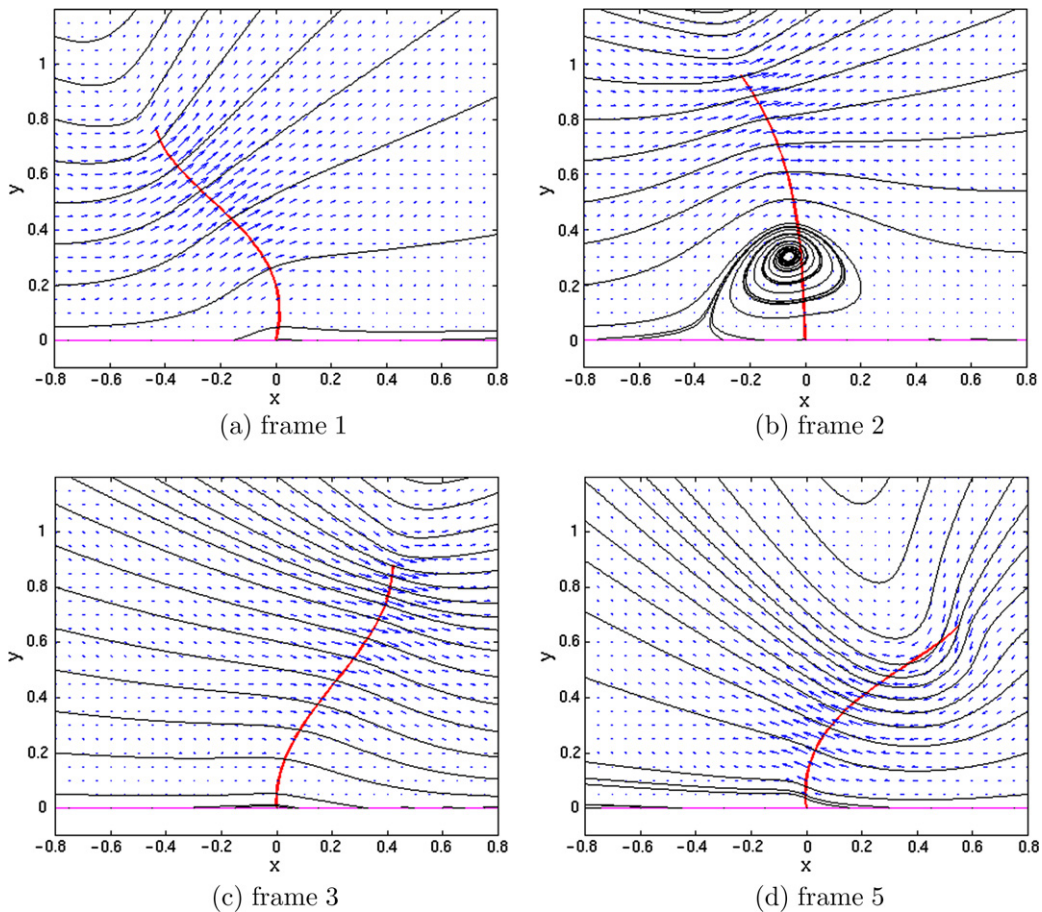


Fig. 6. Flow around a cilium during power stroke. The fluid velocity is shown as a vector field with superimposed streamlines.

5.4. Example 4: the drag on a sphere moving near a wall

The strength of the method of regularized Stokeslets with images is its application to cases in which the forces are distributed along filaments or even scattered points in three dimensions, as presented in the previous examples. In those cases, the standard (singular) Stokeslets yield unbounded flows. If, for example, a filament

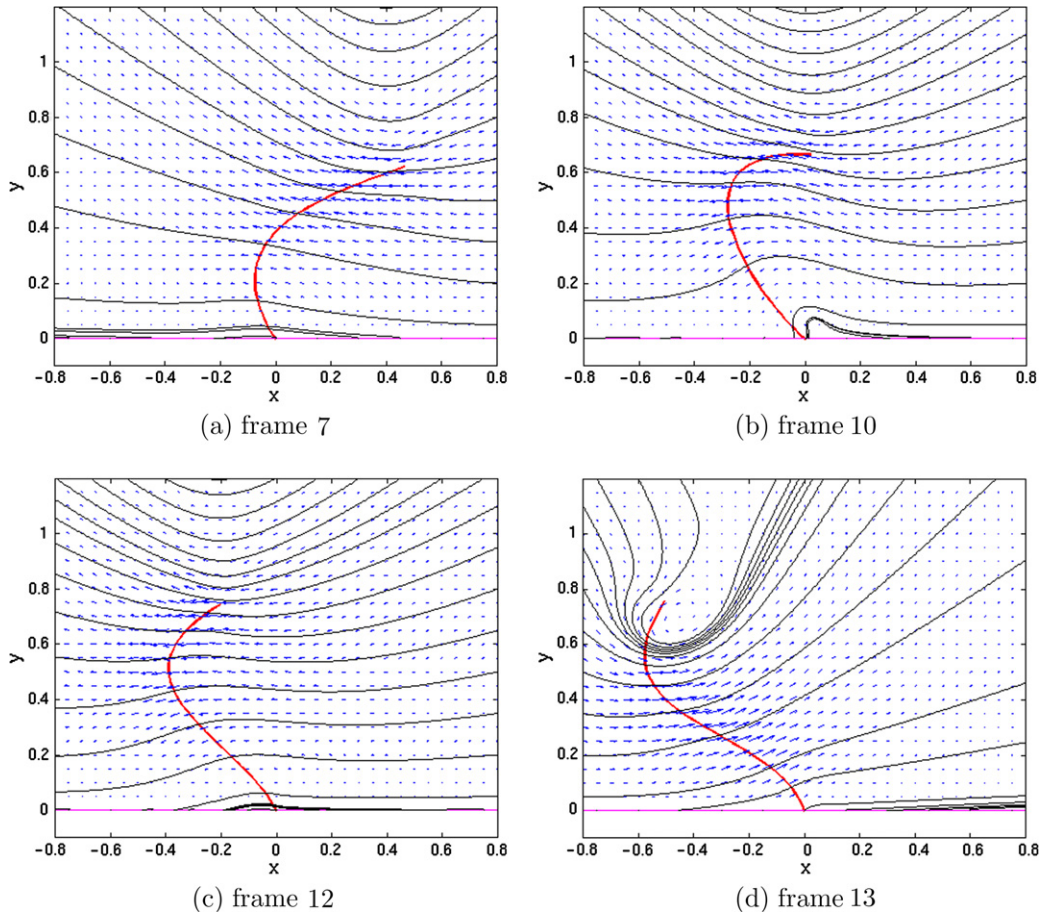


Fig. 7. Flow around a cilium during recovery stroke. The fluid velocity is shown as a vector field with superimposed streamlines.

moving in a Stokes flow represents a thin tubular body, then an alternative is to use a slender body theory [25–27,24,23]. In this example we present the case of forces distributed over the surface of a sphere. We point out that the singular Stokeslet is integrable over surfaces and therefore, there is no need for regularizations. However, we discuss this example using regularization in order to show that our method approximates the solution as the parameter δ is decreased and the discretization of the surface is refined. This also provides a sense of the effect of the regularization parameter.

The motion of a sphere parallel and perpendicular to an infinite rigid wall in a highly viscous fluid has been explored previously by various authors. In 1912, Jeffery [22] developed a general solution of Laplace’s equation for problems in which boundary conditions are given over spherical surfaces. In [29], O’Neill used this formulation while considering a rigid sphere of radius a translating parallel to an infinite plane. Damiano et al. [13] explored the same for a Brinkman half space where it was noted that in the absence of permeability the Brinkman medium is an infinite rigid plane. In the case of a sphere moving perpendicular to an infinite rigid wall, Brenner [6] derived an infinite series solution of the total hydrodynamic force as a correction to Stokes’ law. Jeffrey and Onishi [21] discussed the viscous flow around a cylinder (in two dimensions) that rotates near a plane wall.

In this section we use the image system for the regularized Stokeslets to compute the drag force on spheres moving near a wall as follows. We choose d and place the center of the sphere a distance d from the wall. We then discretize the surface of the sphere using S points and assign all the points the same velocity U . Each point will apply a force to the fluid such that the effect of all the forces is to produce the constant velocity U at all surface points. We then write the velocity of each surface point as the sum in Eq. (21). Those equations

form a $3S \times 3S$ linear system for the surface force components. Once the system is solved, we sum the forces over the surface to determine the net-force F .

For the discretization of the sphere surface, we fix the radius of the sphere to $a = 0.1$ and use spherical coordinates to distribute the points. Given N_ϕ we let $\phi_k = \pi k/N_\phi$ for $k = 0, 1, \dots, N_\phi$. For each value of ϕ_k we set a ring of points

$$(x_j, y_j, z_j) = (a \cos(\phi_k) + d, a \sin(\phi_k) \cos(\theta_j), a \sin(\phi_k) \sin(\theta_j)),$$

where $\theta_j = 2\pi j/N_k$ for $j = 1, 2, \dots, N_k$ and N_k is the smallest integer larger than $2N_\phi \sin(\phi_k)$. This strategy places the points approximately equally spaced on the surface of the sphere. As a representative discretization size we use the parameter h defined as $h = \sqrt{4\pi a^2/S}$, which represents the square root of the average patch of surface area covered by each point.

There is no current convergence theory for the regularized image system but it is known that for Stokeslets alone, the total error is the sum of a regularization error and a discretization error [11]. In that case, appropriate choices of δ are of the form $\delta = Ch^m$ where $0 < m < 1$ and C is a constant. For the examples in this section, we choose $\delta = Ch^{0.9}$ based on reasonable computational results. This choice may not be optimal since a full convergence analysis is required to find the best choice of m .

The resistance of the sphere of radius a translating through a Stokes fluid in the absence of a wall is given by $F_s = 6\pi\mu Ua$, where μ is the fluid viscosity and U is the uniform translational velocity of the sphere. When the sphere translates near the wall, the magnitude of the force F depends on the distance d from the center of the sphere to the wall. Following previous authors, we define a dimensionless force $F^* = \frac{F}{6\pi\mu Ua}$ and present our results in terms of F^* .

5.4.1. Translation parallel to the wall

Table 1 shows the results obtained by O’Neill in [29] and those from our method using four different levels of discretization. For each discretization, we set $\delta = 0.22h^{0.9}$. The gap size in the table is the (smallest) distance between the wall and the sphere surface. Note that the bottom rows of the table are results for the sphere very close to the wall (small gap size) and the convergence as the numerical parameters are refined is slower. In fact, finer discretizations would have to be used to resolve the last two rows since the gap size is smaller than the sphere discretization parameter h . Even in those cases, the method performs well. The errors in the numbers shown in the table can be appreciated in Fig. 8. The figure shows that for most gap sizes, the order of convergence with respect to h is larger than one (curves appear concave up). The two smallest gap sizes show convergence too but finer discretizations are needed to estimate the order.

The component of the force normal to the wall that is exerted on the fluid by the sphere translating parallel to the wall gives important information. Far from the wall, this force is essentially zero; however, for a sphere translating parallel to the wall but close to it, the wall has an attracting effect, as shown in Fig. 9. This is manifested here as a positive component of force (pointing away from the wall) that the sphere must exert on the

Table 1

Comparison of non-dimensional force F^* in the direction of the motion exerted by a sphere of radius $a = 0.1$ translating parallel to the wall

d/a	Gap size	F^* from our method				F^* [29]
		$S = 468$ ($h = 0.0161$)	$S = 812$ ($h = 0.0124$)	$S = 1486$ ($h = 0.00920$)	$S = 2718$ ($h = 0.0068$)	
11013.2	1101.22	0.9933	0.9960	0.9980	0.9991	1.0000
10.0677	0.90677	1.0515	1.0545	1.0567	1.0580	1.0591
3.7622	0.27622	1.1644	1.1681	1.1708	1.1725	1.1738
1.5431	0.05431	1.5459	1.5537	1.5595	1.5632	1.5675
1.1276	0.01276	2.0614	2.0851	2.1056	2.1205	2.1515
1.0453	0.00453	2.4226	2.4621	2.5007	2.5325	2.6475
1.0050	0.00050	3.6581	3.4548	3.3999	3.3945	3.7863

The variable d is the distance from the wall to the center of the sphere. The gap size is the shortest distance between the wall and the sphere surface. The last column shows the forces computed with the analytic formula provided in [29] while columns 3–6 give the forces obtained with our method for increasingly finer discretizations of the sphere surface and $\delta = 0.22h^{0.9}$.

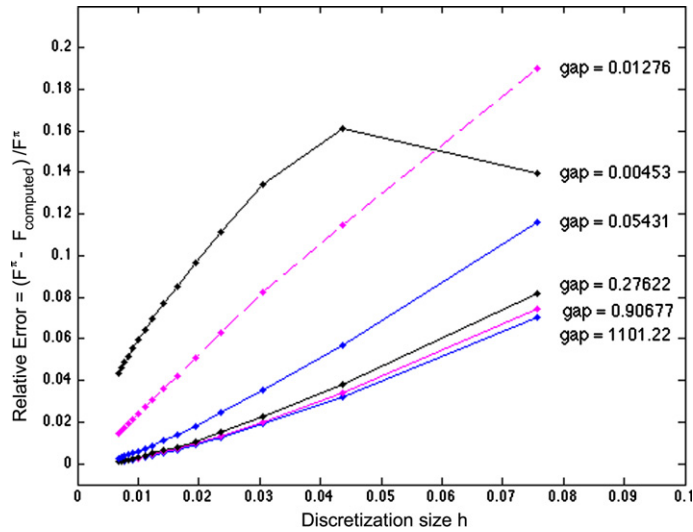


Fig. 8. Relative error in the computed quantities shown in Table 1. The gap is the separation between the wall and the sphere. The curves show the error as a function of discretization size h when $\delta = 0.22h^{0.9}$.

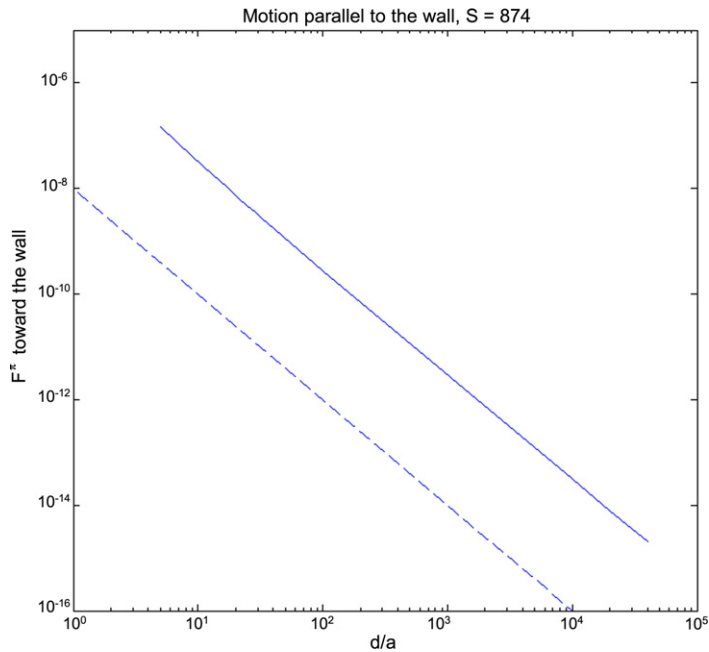


Fig. 9. Component normal to the wall of the (dimensionless) force exerted on the fluid by the sphere translating parallel to the wall as a function of d/a . The dashed line has slope -2 for reference. The parameters used were $S = 874$ ($h = 0.012$) and $\delta = 0.22h^{0.9}$.

fluid in order for the sphere to move parallel to the wall. Without this wall–normal force, like in the case of a sphere dropping under its own weight next to a wall, the sphere velocity would have a component toward the wall and would not simply move parallel to it. Fig. 9 shows that the magnitude of this force is inversely proportional to the square of the distance from the center of the sphere to the wall.

5.4.2. Translation perpendicular to the wall

The analytic expression for the dimensionless force exerted by the sphere on the fluid as it translates perpendicular to the wall is given by [6]

$$F^* = \frac{4}{3} \sinh \alpha \sum_{n=1}^{\infty} \frac{n(n+1)}{(2n-1)(2n+3)} \left[\frac{2 \sinh(2n+1)\alpha + (2n+1) \sinh 2\alpha}{4 \sinh^2(n+\frac{1}{2})\alpha - (2n+1)^2 \sinh^2 \alpha} - 1 \right]. \tag{22}$$

The parameter α is given by $\alpha = \cosh^{-1}(d/a)$. This formula has the property that $\lim_{d \rightarrow \infty} F^* = 1$. For very small values of α , the series converges slowly but Cooley and O’Neill [9] have developed the approximate asymptotic formula

$$F^* \approx \epsilon^{-1} - \frac{1}{5} \ln(\epsilon) + 0.971280 + o(1), \tag{23}$$

where $\epsilon = \cosh(\alpha) - 1 = d/a - 1$.

Table 2 shows the values obtained partly from Eq. (22) and partly from the asymptotic approximation in Eq. (23) as well as the results from our method using four discretizations of the sphere surface. We note first that the force required to translate the sphere perpendicular to the wall is much larger than the force required to translate parallel to the wall, especially at small distances from the wall. This makes the computation more difficult. The results in the table were obtained with $\delta = 0.4h^{0.9}$. The table shows that as long as the surface discretization size is smaller than the gap size, the method gives very good results. For closer distances to the wall, finer discretizations improve the results but the computation requires very fine discretizations. The rows of the table show convergence to the asymptotic values.

Table 2

Comparison of non-dimensional force F^* in the direction of the motion exerted by a sphere of radius $a = 0.1$ translating normal to the wall

d/a	Gap size	F^* from our method				F^* [6,9]
		$S = 468$ ($h = 0.0161$)	$S = 812$ ($h = 0.0124$)	$S = 1486$ ($h = 0.00920$)	$S = 2718$ ($h = 0.0068$)	
11013.2	1101.22	1.0240	1.0187	1.0142	1.0108	1.0000
10.0677	0.90677	1.1556	1.1488	1.1431	1.1388	1.1253
3.7622	0.27622	1.4605	1.4497	1.4408	1.4341	1.4129
1.5431	0.05431	3.2441	3.1952	3.1557	3.1266	3.0361
1.1276	0.01276	10.2872	10.0943	9.9413	9.8021	9.2518
1.0453	0.00453	19.7071	19.4680	20.2478	21.2626	23.6605
1.0050	0.00050	2010.4400	736.6270	326.6780	180.3810	201.8640

The variable d is the distance from the wall to the center of the sphere. The gap size is the shortest distance between the wall and the sphere surface. The last column shows the forces computed with the analytic formula provided in [6] (for $d/a \geq 1.02$) and [9] (for $d/a < 1.02$) while columns 3–6 give the forces obtained with our method for increasingly finer discretizations of the sphere surface and $\delta = 0.4h^{0.9}$.

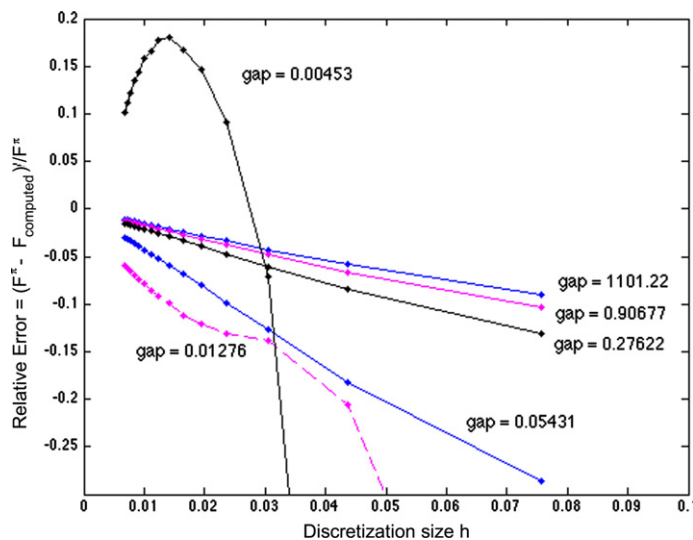


Fig. 10. Relative error in the computed quantities shown in Table 2. The gap is the separation between the wall and the sphere. The curves show the error as a function of discretization size h when $\delta = 0.4h^{0.9}$.

The errors in the table figures is shown in Fig. 10. As in the previous case, when the gap size is resolved by the surface discretization, the method shows convergence rates larger than one. The top curve shows that the error is large when the gap size is not resolved but begins to decrease toward zero once the discretizations are fine enough.

6. Discussion and conclusions

The system of images for the method of regularized Stokeslets has been developed for Stokes flows bounded by an infinite plane wall. Given a regularized Stokeslet in the fluid domain, the images cancel the flow at the wall exactly for any value of the parameter δ . This extends the results in [5] since those expressions are obtained from the regularized images in the limit $\delta \rightarrow 0$. The strength of the method of regularized Stokeslets and its image system is in the simulation of flows generated by point forces or forces distributed along filaments. Those cases are too singular to use forces without regularization. The first three examples shown here fall in this category. When there are scattered point forces like in Examples 1 and 2, the regularization parameter δ may simply give a typical length scale of the particles. The third example uses the method of images to compute the flow around a beating cilium. The motion of the cilium was assumed to be predetermined as given in [18,4]. Although they give the motion of the cilium in a plane, the motion is still three-dimensional in our computations. The cilium was modeled as a curve with a distribution of regularized Stokeslets along it. This cannot be done with the singular Stokeslet formulation. We expect to use a similar approach in connection with a model of the internal force mechanisms of the cilium rather than a predetermined motion.

Our method has been presented for a regularizing function given in Eq. (18) used for the Stokeslet. It turns out that in order for the velocity to vanish at the wall, a different blob must be used for the potential dipole. In addition, the difference of two regularized rotlets, one for each blob, must be included in the images. The results are not restricted to the two blobs used here; they also apply more generally to other choices as long as the two blobs satisfy the statement of Proposition 1. It is not difficult to see that if one chooses a blob for the regularization of the Stokeslets, then the second blob (used for the dipole) can be found by enforcing the Proposition.

In practice, the value of the regularization parameter δ affects the solution and there may be a need to select this parameter in some optimal way. This is usually problem-dependent so it is difficult to give a universal rule; however, in situations where the error in the approximation can be estimated, one can argue for a range of optimal values of δ (see [11]). When the forces are distributed on surfaces or filaments, δ typically must be chosen in relation to the particle separation along the filaments. Typically, one chooses δ to satisfy $\delta = Ch^m$ for some $0 < m < 1$. For the example of the sphere moving near a wall, various values of δ were tested and reasonably good results were obtained with $m = 0.9$. Our results show that the far field velocity is not affected significantly by the specific choice of δ . The near field velocity is sensitive to the choice but only at distances that are on the order of the discretization of the surface. At those distances, the relative location of the discretization nodes matters just as much. In fact, in our examples, we oriented the discretized sphere in such a way that there is a node exactly at the point on the surface nearest to the wall. This is in some sense the most sensitive computation; when we discretized the sphere differently and there was no node at the closest point to the wall, the results in Tables 1 and 2 were much closer to the ones reported in [29,13,6].

Finally, we expect that the regularized image system presented here can be extended to the case of channel flow using techniques like those in [3]. The difficulty with two parallel walls is that since the images of one wall affect the boundary conditions at the other wall, the images themselves require images. This leads to an infinite series of images at increasingly larger distances from the fluid domain. An important observation is that the second generation of images and beyond are all more than one channel width away from the fluid domain. At those distances, the regularization has very little effect and the analysis should be similar to the one in the singular case.

Acknowledgement

This work was supported partly by NSF Grant DMS-0094179.

References

- [1] J.T. Beale, A convergent boundary integral method for three-dimensional water waves, *Math. Comput.* 70 (2001) 977–1029.
- [2] J.T. Beale, A. Majda, High order accurate vortex methods with explicit velocity kernels, *J. Comput. Phys.* 58 (1985) 188–208.
- [3] S. Bhattacharya, J. Blawdziewicz, Image system for Stokes-flow singularity between two parallel planar walls, *J. Math. Phys.* 43 (2002) 5720–5731.
- [4] J. Blake, A model for the micro-structure in ciliated organisms, *J. Fluid Mech.* 55 (1972) 1–23.
- [5] J.R. Blake, A Note on the image system for a Stokeslet in a no-slip boundary, *Proc. Camb. Philos. Soc.* 70 (1971) 303.
- [6] H. Brenner, The slow motion of a sphere through a viscous fluid towards a plane surface, *Chem. Eng. Sci.* 16 (1961) 242–251.
- [7] A. Chorin, A numerical study of slightly viscous flow, *J. Fluid Mech.* 57 (1973) 785–796.
- [8] L. Cisneros, R. Cortez, C. Dombrowski, R. Goldstein, J. Kessler, Fluid dynamics of self-propelled organisms, from individuals to concentrated population, *Exp. Fluids* 43 (2007) 737–753.
- [9] M.D.A. Cooley, M.E. O’Neill, On the Slow motion generated in a viscous fluid by the approach of a sphere to a plane wall or stationary sphere, *Mathematika* 16 (1969) 37–49.
- [10] R. Cortez, The method of regularized Stokeslets, *SIAM J. Sci. Comput.* 23 (4) (2001) 1204–1225 (electronic).
- [11] R. Cortez, L. Fauci, A. Medovikov, The method of regularized Stokeslets in three dimensions: analysis, validation and application to helical swimming, *Phys. Fluids* 17 (2005) 1–14.
- [12] Ricardo Cortez, Michael Minion, The blob projection method for immersed boundary problems, *J. Comput. Phys.* 161 (2) (2000) 428–453.
- [13] E.R. Damiano, D.S. Long, F.H. Khatib-El, T.M. Stace, On the motion of a sphere in a Stokes flow parallel to a Brinkman half-space, *J. Fluid Mech.* 500 (2004) 75–101.
- [14] R. Dillon, L. Fauci, An integrative model of internal axoneme mechanics and external fluid dynamics in ciliary beating, *J. Theor. Biol.* 207 (2000) 415–430.
- [15] C. Dombrowski, L. Cisneros, S. Chatkaew, R. Goldstein, J. Kessler, Self-concentration and large-scale coherence in bacterial dynamics, *Phys. Rev. Lett.* 93 (9) (2004) 098103.
- [16] L. Fauci, A. McDonald, Sperm motility in the presence of boundaries, *Bull. Math. Biol.* 57 (1995) 679–699.
- [17] H. Flores, E. Lobaton, S. Mendez-Diez, S. Tlupova, R. Cortez, A study of bacterial flagellar bundling, *Bull. Math. Biol.* 67 (2005) 137–168.
- [18] G.R. Fulford, J.R. Blake, Muco-ciliary transport in the lung, *J. Theor. Biol.* 121 (1986) 381–402.
- [19] O.H. Hald, Convergence of vortex methods, in: K.E. Gustafson, J.A. Sethian (Eds.), *Vortex Methods and Vortex Motion*, SIAM, 1991, pp. 33–58.
- [20] J.P. Hernandez-Ortiz, C.G. Stoltz, M.D. Graham, Transport and collective dynamics in suspensions of confined swimming particles, *Phys. Rev. Lett.* 95 (2005) 204501.
- [21] D.J. Jeffery, Y. Onishi, The slow motion of a cylinder next to a plane wall, *Quantum J. Mech. Appl. Math.* 34 (1981) 129–137.
- [22] G.B. Jeffery, On a form of the solution of Laplace’s equation suitable for problems relating to two spheres, *Proc. Roy. Soc. Lond., A* 87 (593) (1912) 109–120.
- [23] R.E. Johnson, An improved slender-body theory for stokes flow, *J. Fluid Mech.* 99 (1980) 411–431.
- [24] J.B. Keller, S.I. Rubinow, Slender-body theory for slow viscous flow, *J. Fluid Mech.* 75 (1976) 705–714.
- [25] Sir J. Lighthill, *Mathematical Biofluidynamics*, SIAM, Philadelphia, 1975.
- [26] Sir J. Lighthill, Flagellar hydrodynamics, *SIAM Rev.* 18 (1976) 161–230.
- [27] Sir J. Lighthill, Helical distributions of Stokeslets, *J. Eng. Math.* 30 (1996) 35–78.
- [28] H. Ma, M.D. Graham, Theory of shear-induced migration in dilute polymer solutions near solid boundaries, *Phys. Fluids* 17 (2005) 083103.
- [29] M.E. O’Neill, Slow motion of viscous liquid caused by a slowly moving solid sphere, *Mathematika* 11 (1964) 67–74.
- [30] C.S. Peskin, The immersed boundary method, *Acta Numer.* 11 (2002) 479–517.
- [31] C. Pozrikidis, *Introduction to theoretical and computational fluid mechanics*, Oxford University Press, Oxford, UK, 1997.